PROCEEDINGS OF SCIENCE

Search for $H^{\pm} \to \tau^{\pm}\nu_{\tau}$ with fully hadronic final state in CMS

Alexandros Attikis[*†]
University of Cyprus
E-mail: Alexandros.Attikis@cern.ch

A search for light charged Higgs bosons is presented, conducted using $t\bar{t}$ events with the $t \to bH^{\pm}$ and $H^{\pm} \to \tau^{\pm}\nu_{\tau}$ decay modes, and in the fully hadronic final state. The search was based on $2.3\,\text{fb}^{-1}$ of data, delivered by the LHC and recorded with the CMS detector in 2011, at a centre-of-mass energy $\sqrt{s} = 7\,\text{TeV}$. No excess of events was observed over the expected SM background. Model-independent upper limits were calculated for the $t \to bH^{\pm}$ branching ratio. These limits were translated in the $(m_{H^{\pm}}, \tan\beta)$ parameter space of the MSSM in the maximal mixing scenario ($m_{\text{h}}^{\text{max}}$), excluding a significant region that had previously remained unexplored.

Prospects for Charged Higgs Discovery at Colliders
October 8-11, 2012
Uppsala University Sweden

[*]Speaker.
[†]on behalf of the CMS Collaboration.

PoS(CHARGED 2012)007

1. Introduction

In order to preserve Supersymmetry (SUSY) [1 – 8], the Minimal Supersymmetric Standard Model (MSSM) contains two Higgs doublets, which implies the existence of five physical Higgs states; the CP-even h^0 and H^0, the CP-odd A^0, and the electrically charged H^+ and H^- states [9, 10]. At lowest-order, the MSSM Higgs boson sector is defined by the gauge couplings, the ratio of the two Higgs vacuum expectation values ($\tan\beta = \frac{v_2}{v_1}$), and the mass of the CP-odd Higgs boson (m_{A^0}). Within the Standard Model (SM), top quarks decay promptly to a $W^{\pm}$ boson and a b quark through $t \to bW^+$, and because of lepton universality the branching ratio of $W^{\pm}$ to leptons $\mathrm{BR}(W^{\pm} \to \ell^{\pm}\nu_{\ell})$ is evenly distributed among the three lepton flavours ($\ell^{\pm} = \mathrm{e}^{\pm}, \mu^{\pm}, \tau^{\pm}$). However, if a charged Higgs boson exists with a mass lighter than that of the t quark ($m_{H^{\pm}} \lesssim m_t - m_b$), t quarks can also decay to a $H^{\pm}$ and a b quark via $t \to bH^+$, with a cross-section that depends on the value of $\tan\beta$, as shown in Fig. 1 (a). This opens up the possibility to search for such particles in $t\bar{t} \to bW^{\pm}bH^{\mp}$ and $t\bar{t} \to bH^{\pm}bH^{\mp}$ decays. For small values of $m_{H^{\pm}}$, charged Higgs bosons preferentially decay to a τ lepton and a neutrino through $H^{\pm} \to \tau^{\pm}\nu_{\tau}$ and with $\mathrm{BR}(H^{\pm} \to \tau^{\pm}\nu_{\tau}) \approx 1$, as shown in Fig. 1 (b).

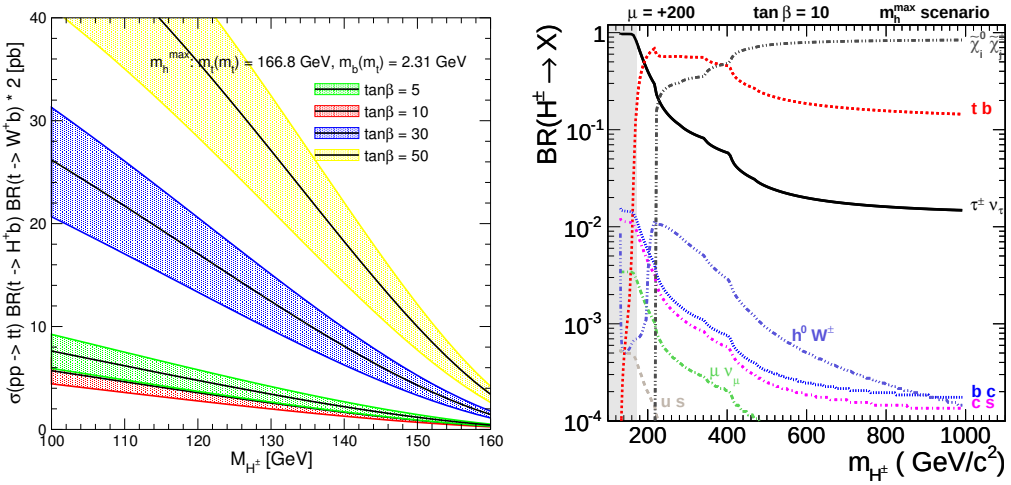

(a) (b)

Figure 1: (a) The production cross-section for light charged Higgs bosons at the LHC for the process $pp \to t\bar{t} \to bH^{\pm}bW^{\mp}$ at $\sqrt{s}$=7 TeV [11]. (b) The decay branching ratio of charged Higgs bosons, as a function of $m_{H^{\pm}}$ and for $\tan\beta = 10$. The shaded area indicates the region where $m_{H^{\pm}} \lesssim (m_t - m_b)$ [12].

The fact that the light charged Higgs boson preferentially decays to a τ lepton implies that, should it exist, the prediction of the τ lepton yield in the decay products of SM $t\bar{t}$ pairs is expected to be altered. Since the dominant process of production of t quarks at the LHC is through $pp \to t\bar{t}$, and given the preferential coupling of light $H^{\pm}$ to τ leptons, searches for light $H^{\pm}$ are conducted using the $t\bar{t} \to bH^{\pm}bW^{\mp}$ and $t\bar{t} \to bH^{\pm}bH^{\mp}$ processes, with the $H^{\pm} \to \tau^{\pm}\nu_{\tau}$ decay mode. An analysis that incorporates three final states, all characterised by missing transverse energy ($E_{\mathrm{T}}^{\mathrm{miss}}$) and multiple jets, was conducted by the Compact Muon Solenoid (CMS) Collaboration and is

documented in Ref. [13]; the fully hadronic final state (τ_h+jets), the semileptonic final states where the τ jet is produced in association with an electron or a muon (τ_h+e, τ_h+μ), and the dilepton final state whereby an electron and a muon are produced (eμ). Two of the three final states involve a τ lepton decaying hadronically (τ jet or τ_h). The study presented here concerns the fully hadronic final state (τ_h+jets), whose dominant production modes are shown in Fig. 2.

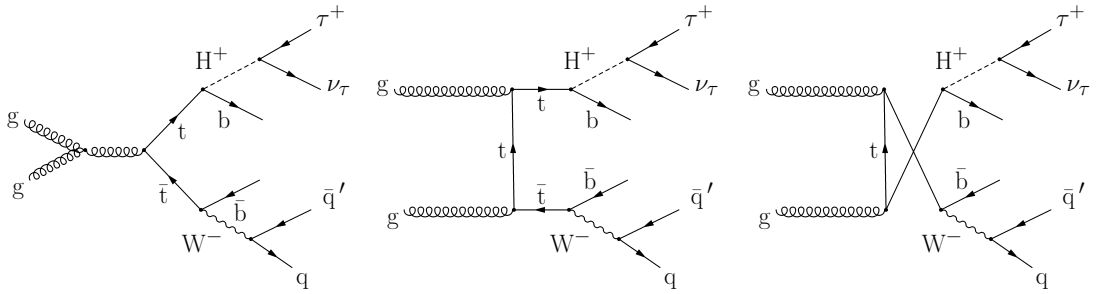

Figure 2: The dominant Feynman diagrams ($\sim 87\%$) for $t\bar{t} \to bH^{\pm}bW^{\mp}$ production at the LHC; gluon-gluon fusion through the (a) s-channel, (b) t-channel, and (c) u-channel [12].

2. The CMS detector, reconstruction, and simulation

The central feature of the CMS apparatus is a superconducting solenoid of 6 m internal diameter, providing a magnetic field of 3.8 T. Within the superconducting solenoid volume are a silicon pixel and strip tracker, a lead tungstate crystal Electromagnetic Calorimeter (ECAL), and a brass/scintillator Hadronic Calorimeter (HCAL). Muons are measured in gas-ionisation detectors embedded in the steel return yoke. Extensive forward calorimetry complements the coverage provided by the barrel and endcap detectors. The ECAL has an energy resolution of better than 0.5% for unconverted photons with transverse energies above 100 GeV. The HCAL, when combined with the ECAL, measures jets with a resolution $\Delta E/E \approx 100\%/\sqrt{E\,[\mathrm{GeV}]} \oplus 5\%$. A right-handed coordinate system is used, with the origin at the nominal interaction point, the x axis pointing to the centre of the LHC, the y axis pointing up (perpendicular to the LHC plane), and the z axis along the anticlockwise-beam direction. The polar angle θ is measured from the positive z axis and the azimuthal angle ϕ is measured in the x-y plane. The Lorentz-invariant pseudorapidity (η) is defined as $\eta = -\ln\left(\tan\frac{\theta}{2}\right)$. A more detailed description of CMS can be found in Ref. [14].

As the CMS detector cannot record every inelastic collision that takes place, it employs a dedicated trigger system [14] that is able to select only interesting events, while also achieving a drastic event rate reduction. This task is accomplished in two steps; the Level-1 (L1) Trigger and High-Level Trigger (HLT). The L1 Trigger is composed of custom-made hardware processors, which use information from the calorimeters and muon detectors to filter events in a fixed time interval of less than 4 μs. The HLT is a software-based filter system, whose task is to decrease the event rate from around 100 kHz to around 300 Hz, before data storage and analysis.

For the reconstruction of the collision events in this analysis, the electrons are reconstructed from clusters of energy deposits in the ECAL which match hits in the silicon tracker [15]. Muons

are reconstructed by performing a simultaneous global track fit to hits in the silicon tracker and the muon system [16]. For composite objects such as jets, τ jets, and $E_{\mathrm{T}}^{\mathrm{miss}}$, the reconstruction is achieved by the use of the Particle Flow (PF) algorithm [17], which combines sub-detector information from the tracker, ECAL, HCAL, and muon systems to reconstruct a particle-based description of the full event. In particular, the anti-k_{T} algorithm [18] with distance parameter of $R = 0.5$ is used for jets, while $E_{\mathrm{T}}^{\mathrm{miss}}$ is defined as the magnitude of the vector sum of the transverse momenta of all PF reconstructed objects in the detector volume (leptons, photons, and hadrons). The tagging of jets originating from the hadronisation of a b quark (b jet) is performed using the Track Counting High Efficiency (TCHE) algorithm [19], which relies on the significance of the impact parameter of tracks and is designed to maximise the efficiency of finding genuine b jets. The identification and reconstruction of τ jets is accomplished with the use of the Hadron plus Strips (HPS) algorithm [20], which considers candidates with one or three charged pions and up to two neutral pions. The τ jet isolation is based on a cone of $\Delta R = \sqrt{\Delta\phi^2 + \Delta\eta^2} = 0.5$ around the reconstructed τ jet momentum direction. Within this isolation cone, besides the τ jet constituents no charged hadrons with $p_{\mathrm{T}} > 0.5\,\mathrm{GeV}/c$ and no photons with $E_{\mathrm{T}} > 0.5\,\mathrm{GeV}$ are allowed to be present.

Simulated events are processed through the full detector simulation based on GEANT4 [21], followed by a detailed trigger emulation and the CMS event reconstruction. Several minimum-bias events are superimposed upon the hard interactions to simulate pileup. The simulated events are weighted according to the measured distribution of the number of interaction vertices, and are normalised by their cross-section to the total integrated luminosity of the collision data. The PYTHIA6 [22] parameters for the underlying event are set according to Tune Z2 [23], which incorporates fine-tuning to parameters related to colour re-connection and parton showering [24].

3. Event selections

The present analysis is based on an integrated luminosity of $2.3\,\mathrm{fb}^{-1}$ of data recorded with the CMS detector in 2011, with an LHC instantaneous luminosity of up to $5 \times 10^{33}\mathrm{cm}^{-2}\,\mathrm{s}^{-1}$. The collision events are selected by employing a single τ jet $+ E_{\mathrm{T}}^{\mathrm{miss}}$ trigger, chosen due to its relatively low rate and its effectiveness in suppressing the dominant QCD multijet background. In particular, the trigger requires the presence of a τ jet with transverse momentum $p_{\mathrm{T}} > 35\,\mathrm{GeV}/c$ (leading-track $p_{\mathrm{T}} > 20\,\mathrm{GeV}/c$) and a large calorimetric $E_{\mathrm{T}}^{\mathrm{miss}}$ ($> 60\,\mathrm{GeV}$). The offline event selections require that no isolated electrons or muons with $p_{\mathrm{T}} > 15\,\mathrm{GeV}/c$ are present (isolated lepton veto), in order to ensure orthogonality with the semileptonic and dilepton final states. In addition, the presence of a well identified and tightly isolated τ jet is required, with $p_{\mathrm{T}} > 40\,\mathrm{GeV}/c$ and within $|\eta| < 2.1$. Only τ jet candidates consisting of exactly one charged hadron (one-prong) with track $p_{\mathrm{T}} > 20\,\mathrm{GeV}/c$ are considered. In order to enhance the signal with respect to background events with $W^{\pm} \to \tau^{\pm}\nu_{\tau}$ decays, the τ helicity correlations are exploited by setting a lower bound on $R_{\tau} = p^{\text{ldg. trk.}}/p^{\tau\text{ jet}} > 0.7$, where $p^{\text{ldg. trk.}}$ is the momentum of the leading charged particle [25, 26]. In this way, the different polarisation of τ leptons originating from $H^{\pm}$ (scalar) or $W^{\pm}$ (vector) decays is taken into account. At least 3 other jets with $p_{\mathrm{T}} > 30\,\mathrm{GeV}/c$ and $|\eta| < 2.4$ are also required, with at least one of them tagged as a b jet. In order to suppress the QCD multijet background, a large $E_{\mathrm{T}}^{\mathrm{miss}}$ requirement is imposed on the selected events ($E_{\mathrm{T}}^{\mathrm{miss}} > 50\,\mathrm{GeV}$), while the $E_{\mathrm{T}}^{\mathrm{miss}}$ and τ jet

objects must be azimuthally separated by an angle $\Delta\phi(\tau \text{ jet}, E_{\mathrm{T}}^{\mathrm{miss}}) < 160^{\circ}$. After all selection requirements the transverse mass (m_{T}) is reconstructed from the τ jet and $E_{\mathrm{T}}^{\mathrm{miss}}$ vectors, providing additional discrimination between signal and background events.

4. Measurements, results, and systematics uncertainties

The single τ jet $+ E_{\mathrm{T}}^{\mathrm{miss}}$ trigger efficiency is measured from data, separately for the τ part and the $E_{\mathrm{T}}^{\mathrm{miss}}$ part. The efficiency of the τ part of the trigger is measured in three separate runs, by the use of single isolated μ trigger and the Tag-and-Probe technique. More specifically, $Z^0/\gamma^* \to \tau^{\pm}\tau^{\mp}$ events are selected with the additional requirement that one τ lepton decays to a μ (tag) and the other decays hadronically (probe). The offline selections require that exactly one good muon and one well identified τ jet are present. Furthermore, the transverse and invariant mass requirements $m_{\mathrm{T}}(\mu, E_{\mathrm{T}}^{\mathrm{miss}}) < 40\,\mathrm{GeV}/c^2$ and $m(\mu, \tau \text{ jet}) < 80\,\mathrm{GeV}/c^2$ are used to suppress $W+$jets and $Z^0/\gamma^* \to \mu^{\pm}\mu^{\mp}$ events, respectively. The overall L1+HLT efficiency, as a function of offline τ jet p_{T}, is shown in Fig. 3 (a) for a selected run period. The difference in the efficiencies between data and simulation is taken into account by applying scale factors to simulation. In Fig. 3 (b) the efficiency of the $E_{\mathrm{T}}^{\mathrm{miss}}$ part of the single τ jet $+ E_{\mathrm{T}}^{\mathrm{miss}}$ trigger is shown, as a function of offline $E_{\mathrm{T}}^{\mathrm{miss}}$. This efficiency is measured from the calorimetry $E_{\mathrm{T}}^{\mathrm{miss}}$ object, which was found to be a good approximation of HLT $E_{\mathrm{T}}^{\mathrm{miss}}$, using events where single μ triggers are fired and with signal-like topologies. The efficiencies for data and simulation are in agreement within 10% in the region of interest ($E_{\mathrm{T}}^{\mathrm{miss}} > 50\,\mathrm{GeV}$) and thus no scale factors are used, and instead a 10% uncertainty is added to the τ part of the trigger.

The background processes related to the analysis can be separated into three main categories; QCD multijet, Electroweak (EWK)+$t\bar{t}$ τ and EWK+$t\bar{t}$ no-τ. Their estimation is explained in detail in Refs. [12, 27, 28]. The dominant reducible background arises from QCD multijet events with large $E_{\mathrm{T}}^{\mathrm{miss}}$ and jets mimicking the signature of a τ jet or being misidentified as b jets. This background is largely suppressed by employing tight τ jet isolation, large $E_{\mathrm{T}}^{\mathrm{miss}}$, and the $\Delta\phi(\tau \text{ jet}, E_{\mathrm{T}}^{\mathrm{miss}}) < 160^{\circ}$ requirement. It is measured from data by employing factorisation methods on events passing the single τ jet $+ E_{\mathrm{T}}^{\mathrm{miss}}$ trigger, as QCD multijet events strongly dominate at this selection step. The other two background categories consist of EWK processes, namely $W+$jets, $Z+$jets, di-boson (WW, WZ, ZZ), Drell-Yan ($Z^0/\gamma^* \to \ell\ell$) as well as single-top (s-, t- and tW-channels) and SM $t\bar{t}$ production, with the $W+$jets and SM $t\bar{t}$ particularly dominant. This largely irreducible background is divided into the EWK+$t\bar{t}$ τ and EWK+$t\bar{t}$ no-τ type backgrounds. The EWK+$t\bar{t}$ τ background refers to events where at least one τ lepton is in the final state and within the acceptance of the analysis ($p_{\mathrm{T}} > 40\,\mathrm{GeV}/c, |\eta| < 2.1$). It is measured from data using events resembling a $t\bar{t}$ topology and containing an energetic muon and jets, by transforming the muon into a simulated τ jet with the τ-embedding method. The EWK+$t\bar{t}$ no-τ background refers to events with no τ leptons in the final state, or with a τ lepton outside the acceptance. This minor background can pass the selection requirements due to electrons, muons and jets being misidentified as τ jets. As this is a minor background ($\sim 5\%$ of event yield) it is taken from simulation.

The use of data-driven techniques to determine the QCD multijet and EWK+$t\bar{t}$ τ processes allows for key kinematical distributions to be extracted from data, in successive steps of the event selections. In Fig. 4 (a), the distribution of the number of selected jets is shown, after the τ jet

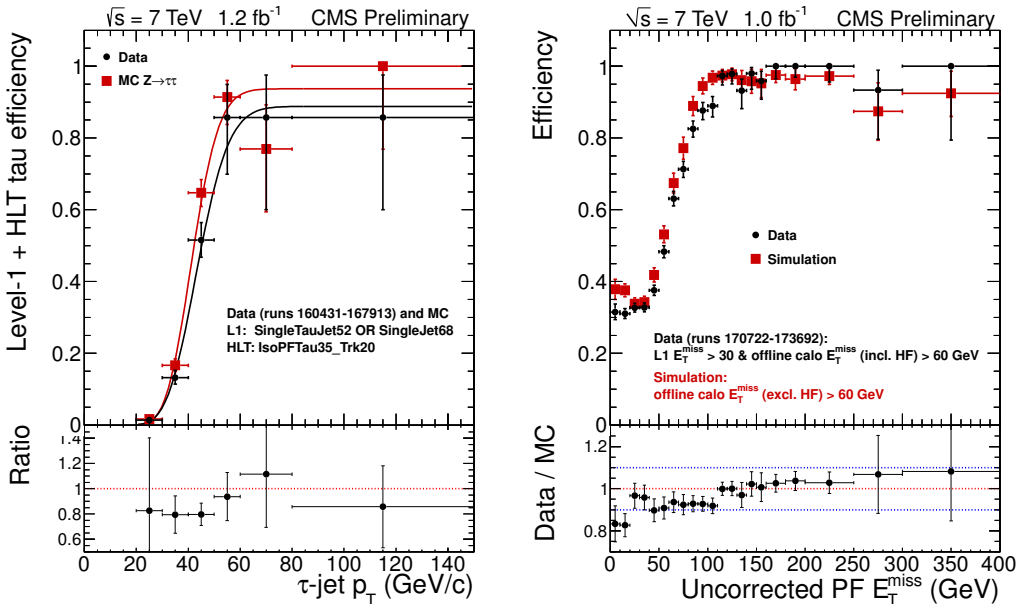

(a) (b)

Figure 3: Overall L1+HLT efficiency for data and simulated samples for (a) the τ part of the single τ jet $+ E_{\mathrm{T}}^{\mathrm{miss}}$ trigger as measured for one of the three 2011 run periods and (b) the $E_{\mathrm{T}}^{\mathrm{miss}}$ part of the single τ jet $+ E_{\mathrm{T}}^{\mathrm{miss}}$ trigger as measured from the requirement that calorimeter $E_{\mathrm{T}}^{\mathrm{miss}} > 60\,\mathrm{GeV}$ [12, 27].

identification, isolated lepton veto, and ≥ 3 jets requirements. The observed and expected background events are found to agree within statistical uncertainties in the first two bins, which are the most dominant ones statistics-wise. At the same selection step the $E_{\mathrm{T}}^{\mathrm{miss}}$ distribution, presented in Fig. 4 (b), shows that the number of observed and expected background events are within statistical uncertainty over the full $E_{\mathrm{T}}^{\mathrm{miss}}$ spectrum, supporting the case that the dominant backgrounds are described well by the analysis. A prominent feature of the event topology is the transitional region at $E_{\mathrm{T}}^{\mathrm{miss}} \approx 90\,\mathrm{GeV}$, where the EWK+$t\bar{t}$ τ background overtakes the QCD multijet background as the dominant process.

As it can be seen in Fig. 5 (a), the inclusion of the $E_{\mathrm{T}}^{\mathrm{miss}} > 50\,\mathrm{GeV}$ selection to the aforementioned set of selections, results in a small excess of observed events that contain exactly 1 b jet. The remaining b jet spectrum appears to show good agreement within statistical uncertainty between the number of observed and expected background events. This slight excess appears to be carried over to the $\Delta\phi\left(\tau\,\mathrm{jet}, E_{\mathrm{T}}^{\mathrm{miss}}\right)$ distribution, shown in Fig. 5 (b), where a distinct separation between QCD multijet and EWK+$t\bar{t}$ τ processes is clearly visible. For QCD multijet events the $\Delta\phi\left(\tau\,\mathrm{jet}, E_{\mathrm{T}}^{\mathrm{miss}}\right)$ distribution structure can be understood by the production of back-to-back jets, with one of the two jet energies being mismeasured and one jet falsely identified as τ jet. In this configuration the $E_{\mathrm{T}}^{\mathrm{miss}}$ vector points to the same (opposite) direction as the direction of the undermeasured (overmeasured) jet. For EWK+$t\bar{t}$ τ events in which the τ lepton is produced boosted, as is the case for $t\bar{t}$ events for example, the neutrino and the τ lepton decay products are collinear, and thus the angle between the reconstructed τ jet and $E_{\mathrm{T}}^{\mathrm{miss}}$ is expected to be small. However,

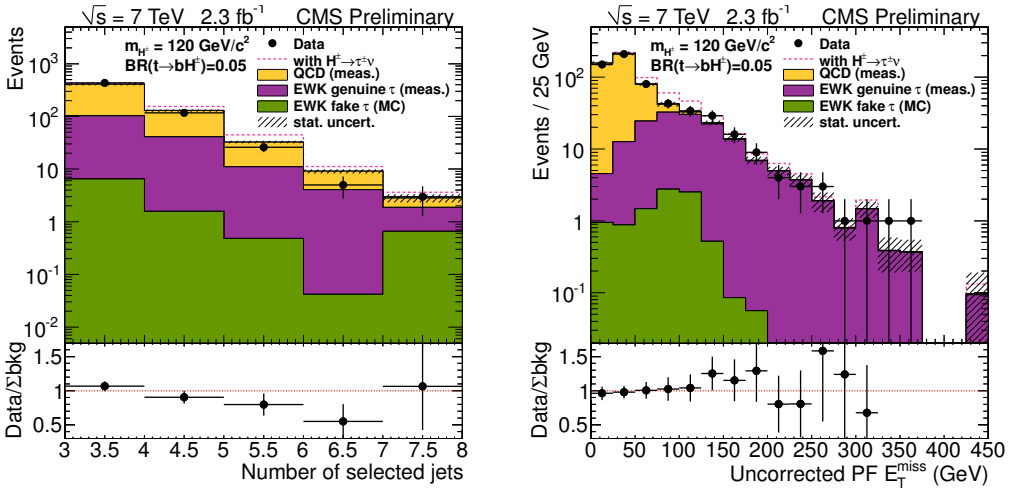

(a) (b)

Figure 4: (a) Distribution of the number of selected jets after τ jet identification, isolated lepton veto, and ≥ 3 jets requirements [12]. (b) Distribution of $E_{\mathrm{T}}^{\mathrm{miss}}$ after the τ jet identification, isolated lepton veto, and ≥ 3 jets requirements. The QCD multijet and EWK+$t\bar{t}$ τ backgrounds are shown as measured from data, while the EWK+$t\bar{t}$ no-τ background is estimated from simulation. The expected event yield in the presence of the $t \to bH^{\pm}$, $H^{\pm} \to \tau^{\pm}\nu_{\tau}$ decays is shown as the dashed red line for $m_{H^{\pm}} = 120\,\mathrm{GeV}/c^2$ and assuming $\mathrm{BR}(t \to bH^{\pm}) = 0.05$ and $\mathrm{BR}(H^{\pm} \to \tau^{\pm}\nu_{\tau}) = 1$.

effects such as semileptonic b quark decays and jet mismeasurements can have a smearing effect on the expected $\Delta\phi\left(\tau\,\mathrm{jet}, E_{\mathrm{T}}^{\mathrm{miss}}\right)$ distribution which results in the structure shown here. In Fig. 5 (c), the total event yield after each selection step is shown. A distinct feature is that, although QCD multijet events is the dominant background, it can nevertheless be greatly suppressed, unlike the EWK+$t\bar{t}$ τ background which remains largely irreducible. The EWK+$t\bar{t}$ no-τ background remains negligible throughout the selection steps, while the presence of a signal is persistently expected to be manifested as an excess of events.

The number of observed and expected background events after all selections is summarised in Table 1, along with the total signal yield expected from $t\bar{t} \to bW^{\pm}bH^{\mp}$ and $t\bar{t} \to bH^{\pm}bH^{\mp}$ for $m_{H^{\pm}} = 120\,\mathrm{GeV}/c^2$, and assuming $\mathrm{BR}(t \to bH^{\pm}) = 0.05$ and $\mathrm{BR}(H^{\pm} \to \tau^{\pm}\nu_{\tau}) = 1$. The quoted systematic uncertainties are due to multiple sources. The uncertainty on the Jet Energy Scale (JES), Jet Energy Resolution (JER) and $E_{\mathrm{T}}^{\mathrm{miss}}$ is estimated as described in Ref. [29]. The uncertainty on the τ jet energy is taken to be 3% [20]. The theoretical uncertainties on the signal and background cross sections is accounted for, as is the uncertainty on pileup modelling due to the re-weighting of simulated events according to the measured distribution of the number of vertices. The statistical limitation of the simulated samples used is accordingly included, as is the statistical uncertainty of the data samples. A 2.2% uncertainty is adopted for the integrated luminosity [30]. The uncertainty on trigger efficiencies, used in the EWK+$t\bar{t}$ τ background estimate, is calculated by adding in quadrature the τ part and $E_{\mathrm{T}}^{\mathrm{miss}}$ part uncertainties. The data-to-simulation correction factors are used for the signal and EWK+$t\bar{t}$ no-τ estimates. The uncertainty in the application of the isolated lepton veto is also accounted for, as estimated from the uncertainty in the lepton reconstruction,

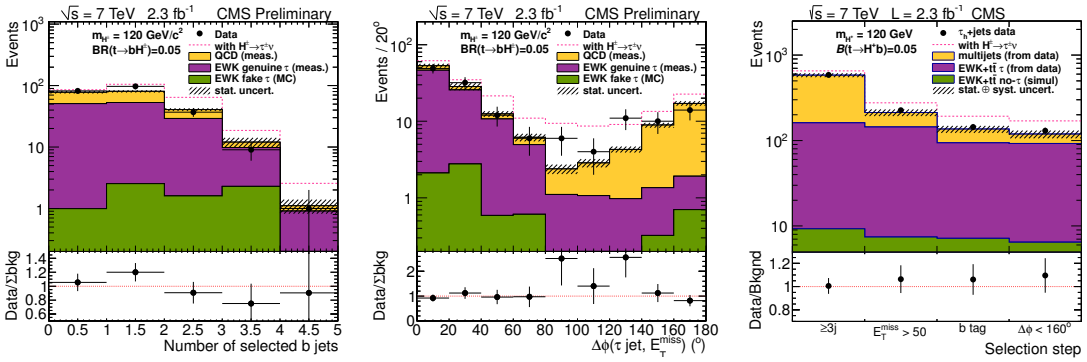

(a) (b) (c)

Figure 5: (a) Number of selected b jets after τ jet identification, isolated lepton veto, ≥ 3 jets, and $E_{\mathrm{T}}^{\mathrm{miss}} > 50\,\mathrm{GeV}$ requirements. (b) The $\Delta\phi\left(\tau\,\mathrm{jet}, E_{\mathrm{T}}^{\mathrm{miss}}\right)$ distribution after τ jet, lepton veto, ≥ 3 jets, $E_{\mathrm{T}}^{\mathrm{miss}} > 50\,\mathrm{GeV}$, and ≥ 1 b jet requirements. (c) The event yield after each selection step. The figure style is the same as in Fig. 4.

identification, and isolation efficiencies of 2% (1%) for electrons (muons) measured using $Z^0 \to \ell^{\pm}\ell^{\mp}$ ($\ell = \mathrm{e}, \mu$) events. The uncertainty on the efficiency of τ jet identification is estimated to be 6%. The uncertainty on the rate of misidentification of a jet as a τ jet, or of a lepton (e, μ) as a τ jet is estimated to be 15% [20]. The uncertainty on the efficiency of b-tagging is taken to be 5.4%, while the uncertainty on the rate of misidentification of a jet as a b jet is taken to be 10% [31]. The QCD multijet uncertainty is evaluated by error propagation, while for the EWK+$t\bar{t}$ τ background the uncertainty accounts for the single τ jet + $E_{\mathrm{T}}^{\mathrm{miss}}$ trigger efficiency, the τ jet energy scale, the τ jet identification efficiency, and the statistical uncertainty of the samples.

Table 1: Summary of the expected and observed event yields, for $2.3\,\mathrm{fb}^{-1}$ of data.

Process	Events	Statistical	Systematic
$H^{\pm}H^{\mp} + H^{\pm}W^{\mp}$	51	± 4	± 8
EWK+$t\bar{t}$ τ (data-driven)	85.8	± 3.6	± 11.2
QCD multijet (data-driven)	26	± 2	± 1
EWK+$t\bar{t}$ no-τ (simulation)	6.4	± 3.1	± 3.3
Expected from SM	119	± 5	± 12
Observed in data	130		

5. Exclusion limits

The light charged Higgs boson transverse mass is used to extract upper limits on the branching ratio $\mathrm{BR}(t \to bH^{\pm})$, which are calculated with the modified frequentist CLs criterion, using a test statistic on the profile likelihood ratio [32]. All associated systematic uncertainties are incorporated in the form of nuisance parameters. The transverse mass $m_{\mathrm{T}}(\tau\,\mathrm{jet}, E_{\mathrm{T}}^{\mathrm{miss}})$ distribution after all selections is shown in Fig. 6. The expected background events are found to accurately describe the distributions observed in the data, and to be in agreement within the total uncertainties for the majority

of the $m_{\mathrm{T}}(\tau\ \mathrm{jet}, E_{\mathrm{T}}^{\mathrm{miss}})$ spectrum. The EWK+$t\bar{t}$ τ background appears to be separable and largely irreducible, while the EWK+$t\bar{t}$ no-τ has a negligible contribution. The QCD multijet background has a two-bump structure, with one of them residing in the region of $m_{\mathrm{T}}(\tau\ \mathrm{jet}, E_{\mathrm{T}}^{\mathrm{miss}}) \simeq 100\,\mathrm{GeV}$, thus obscuring the Jacobian peak expected from signal processes. This effect, which was identified to originate from mismeasured back-to-back jets, is found to be significantly suppressed by the use of the $\Delta\phi\left(\tau\ \mathrm{jet}, E_{\mathrm{T}}^{\mathrm{miss}}\right) < 160^{\circ}$ requirement. The small excess of data events that is visible in the region $m_{\mathrm{T}}(\tau\ \mathrm{jet}, E_{\mathrm{T}}^{\mathrm{miss}}) \approx 100\,\mathrm{GeV}$ persists for even tighter requirements on $\Delta\phi\left(\tau\ \mathrm{jet}, E_{\mathrm{T}}^{\mathrm{miss}}\right)$, suggesting that it is unlikely that it originates from QCD multijet processes.

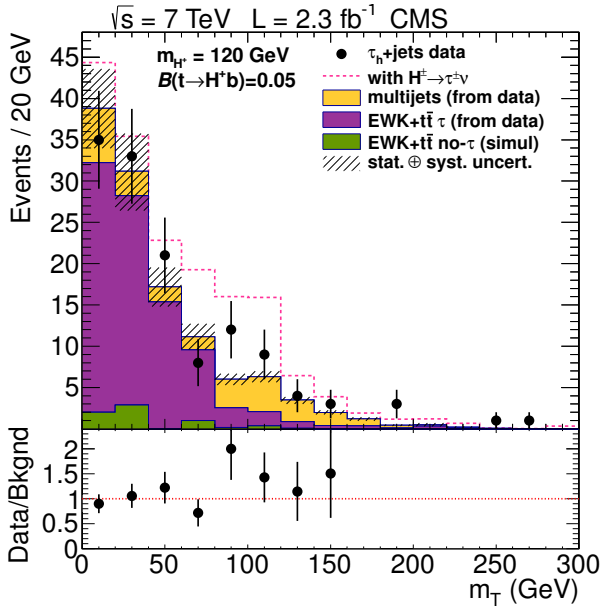

Figure 6: The transverse mass $m_{\mathrm{T}}(\tau\ \mathrm{jet}, E_{\mathrm{T}}^{\mathrm{miss}})$ distribution after all selections, used in extracting the upper limits on $\mathrm{BR}(t \to bH^{\pm})$. The figure style is the same as in Fig. 4.

The full set of systematic uncertainties is used as input to the exclusion limit calculation. The background and signal uncertainties is modelled with a log-normal probability distribution function and their correlations are taken into account. The uncertainties on the transverse mass shapes for the QCD multijet and EWK+$t\bar{t}$ τ backgrounds, which were derived from data, are evaluated by taking into account the corresponding uncertainty in every bin of the m_{T} distribution [12, 27]. For the signal and the small EWK+$t\bar{t}$ no-τ background the m_{T} shape uncertainty in the JES +JER +$E_{\mathrm{T}}^{\mathrm{miss}}$ scale is evaluated from simulation. The 95% CL model-independent upper limits on $\mathrm{BR}(t \to bH^{\pm})$ are shown in Fig. 7 (a). The observed and expected limits are found to lie in the range $2.2-7.3\%$ and $1.5-5.2\%$, respectively, for the mass range $80\,\mathrm{GeV}/c^2 \leq m_{H^{\pm}} \leq 160\,\mathrm{GeV}/c^2$. The FeynHiggs [33] software is used to calculate $\mathrm{BR}(t \to bH^{\pm})$ and $\mathrm{BR}(H^{\pm} \to \tau^{\pm}\nu_{\tau})$ for various $\tan\beta$ values, and thus transform the model-independent upper limits to exclusion regions in the MSSM parameter space. The corresponding exclusion region in the MSSM $(m_{H^{\pm}}, \tan\beta)$ plane is presented in Fig. 7 (b), for the $m_{\mathrm{h}}^{\mathrm{max}}$ scenario and for $\mu = 200\,\mathrm{GeV}$.

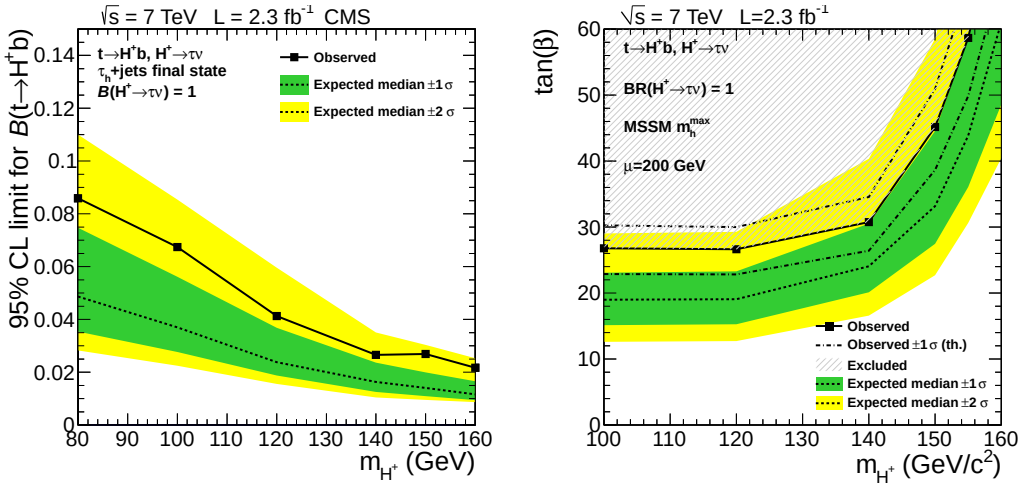

(a) (b)

Figure 7: (a) Model-independent upper limits on BR($t \to bH^{\pm}$), as a function of $m_{H^{\pm}}$. (b) The exclusion region in the MSSM $(m_{H^{\pm}}, \tan\beta)$ parameter space for the $m_{\mathrm{h}}^{\mathrm{max}}$ scenario and with $\mu = 200\,\mathrm{GeV}$ [12]. The one- and two- standard deviation uncertainty bands around the expected limits are also shown.

6. Summary

The present analysis deals with the search for light charged Higgs bosons in $t\bar{t}$ events with the $t \to bH^{\pm}$ and $H^{\pm} \to \tau^{\pm}\nu_{\tau}$ decay modes, in the fully hadronic final state. A total of $2.3\,\mathrm{fb}^{-1}$ of data is used, selected with a single τ jet $+ E_{\mathrm{T}}^{\mathrm{miss}}$ trigger. The offline event selections require the presence of an isolated and well identified τ jet ($p_{\mathrm{T}} > 40\,\mathrm{GeV}/c$ and $|\eta| < 2.1$), at least 3 jets ($p_{\mathrm{T}} > 30\,\mathrm{GeV}/c$ and $|\eta| < 2.4$) of which at least one is tagged as a b jet, $E_{\mathrm{T}}^{\mathrm{miss}} > 50\,\mathrm{GeV}$ and $\Delta\phi(\tau\,\mathrm{jet}, E_{\mathrm{T}}^{\mathrm{miss}}) < 160^{\circ}$. Events with isolated electrons or muons are rejected. The dominant backgrounds are found to be QCD multijet and EWK+$t\bar{t}$ τ processes, both of which are determined from data. The EWK+$t\bar{t}$ no-τ background is found to be small and is thus evaluated from simulation. After all selections the transverse mass $m_{\mathrm{T}}(\tau\,\mathrm{jet}, E_{\mathrm{T}}^{\mathrm{miss}})$ is employed in a binned maximum likelihood ratio fit to the data, to extract model-independent upper limits on BR($t \to bH^{\pm}$). The observed and expected upper limits are found to be $2.2 - 7.3\%$ and $1.5 - 5.2\%$, respectively, for $80\,\mathrm{GeV}/c^2 \leq m_{H^{\pm}} \leq 160\,\mathrm{GeV}/c^2$. These limits are transformed to the $(m_{H^{\pm}}, \tan\beta)$ plane of the MSSM maximal mixing scenario $m_{\mathrm{h}}^{\mathrm{max}}$, and are found to exclude a significant region of the parameter space that had previously remained unexplored.

Acknowledgments

The author would like to thank the Cyprus Research Promotion Foundation's Framework Programme for Research, Technological Development and Innovation 2008 (DESMH 2008), which is co-funded by the Republic of Cyprus and the European Regional Development Fund.

References

[1] Pierre Fayet. *Supergauge Invariant Extension of the Higgs Mechanism and a Model for the Electron and Its Neutrino*. Nucl. Phys. **B90**, 104 (1975).

[2] Pierre Fayet. *Supersymmetry and Weak, Electromagnetic and Strong Interactions*. Phys. Lett. **B64**, 159 (1976).

[3] Pierre Fayet. *Spontaneously Broken Supersymmetric Theories of Weak, Electromagnetic and Strong Interactions*. Phys. Lett. **B69**, 489 (1977).

[4] Savas Dimopoulos and Howard Georgi. *Softly Broken Supersymmetry and SU(5)*. Nucl. Phys. **B193**, 150 (1981).

[5] N. Sakai. *Naturalness in Supersymmetric Guts*. Z. Phys. **C11**, 153 (1981).

[6] Kenzo Inoue, Akira Kakuto, Hiromasa Komatsu and Seiichiro Takeshita. *Low-Energy Parameters and Particle Masses in a Supersymmetric Grand Unified Model*. Prog. Theor. Phys. **67**, 1889 (1982). Revised version.

[7] Kenzo Inoue, Akira Kakuto, Hiromasa Komatsu and Seiichiro Takeshita. *Aspects of Grand Unified Models with Softly Broken Supersymmetry*. Prog. Theor. Phys. **68**, 927 (1982).

[8] Kenzo Inoue, Akira Kakuto, Hiromasa Komatsu and Seiichiro Takeshita. *Renormalization of Supersymmetry Breaking Parameters Revisited*. Prog. Theor. Phys. **71**, 413 (1984).

[9] Abdelhak Djouadi. *The anatomy of electro-weak symmetry breaking. II. The Higgs bosons in the minimal supersymmetric model*. Phys. Rept. **459**, 1 (2008).

[10] John F. Gunion, Howard E. Haber, Gordon L. Kane and Sally Dawson. *The Higgs Hunters' Guide*. Front.Phys. **80**, 1 (2000).

[11] LHC Higgs Cross Section Working Group, S. Dittmaier, C. Mariotti, G. Passarino and R. Tanaka (Eds.). *Handbook of LHC Higgs Cross Sections: 2. Differential Distributions*. CERN-2012-002 (CERN, Geneva, 2012).

[12] Alexandros Attikis. *Search for light charged Higgs bosons with the $H^{\pm} \to \tau^{\pm}\nu_{\tau}$ decay in the fully hadronic final state*. PhD thesis University of Cyprus 20012. CMS TS-2012/033.

[13] Serguei Chatrchyan et al. *Search for a light charged Higgs boson in top quark decays in pp collisions at $\sqrt{s}$ = 7 TeV*. Journal of High Energy Physics **2012**, 1–38 (2012). 10.1007/JHEP07(2012)143.

[14] S. Chatrchyan et al. *The CMS experiment at the CERN LHC*. JINST **03**, S08004 (2008).

[15] *Electron reconstruction and identification at $\sqrt{s}$ =7 TeV*. CMS Physics Analysis Summary **CMS-PAS-EGM-10-004** (2010).

[16] *Performance of muon identification in pp collisions at $\sqrt{s}$ = 7 TeV*. CMS Physics Analysis Summary **CMS-PAS-MUO-10-002** (2010).

[17] *Commissioning of the particle flow reconstruction in minimum-bias and jet events from pp collisions at 7 TeV*. CMS Physics Analysis Summary **CMS-PAS-PFT-10-002** (2010).

[18] M. Cacciari, G. P. Salam and G. Soyez. *The anti-k_T jet clustering algorithm*. JHEP **04**, 063 (2008).

[19] CMS Collaboration. *CMS Commissioning of b-jet identification with pp collisions at $\sqrt{s}$ = 7 TeV*. CMS PAS **BTV-11-001** (2011).

[20] *Performance of τ-lepton reconstruction and identification in CMS*. JINST **07**, P01001 (2012).

[21] S. Agostinelli et al. *Geant4 – A simulation Toolkit*. Nucl. Inst. Meth. A **506**, 250–303 (2003).

[22] T Sjostrand, L Lonnblad, S Mrenna and P Skands. *Pythia 6.3 Physics and Manual*. LU TP **03-38** (2003).

[23] *Measurement of the Underlying Event Activity at the LHC with at $\sqrt{s}$ = 7 TeV and Comparison with $\sqrt{s}$ = 0.9 TeV*. JHEP **2011** (9), 109 (9 2011).

[24] CMS Collaboration. *Measurement of the Underlying Event Activity at the LHC with $\sqrt{s}$=7 TeV*. CMS PAS **QCD-10-010** (2010).

[25] D. P. Roy. *The Hadronic tau decay signature of a heavy charged Higgs boson at LHC*. Phys. Lett. **B459**, 607 (1999).

[26] Monoranjan Guchait, Ritva Kinnunen and D. P. Roy. *Signature of heavy charged Higgs boson at LHC in the 1 and 3 prong hadronic tau decay channels*. Eur. Phys. J. **C52**, 665–672 (2007).

[27] M. J. Kortelainen. *Search for a Light Charged Higgs Boson in the CMS Experiment in pp Collisions at $\sqrt{s}$ = 7 TeV*. PhD thesis University of Helsinki 2012. HIP-2012-06.

[28] M. J. Kortelainen. *Data-driven background estimation in CMS*. PoS **CHARGED2012**. submitted.

[29] CMS Collaboration. *Determination of the jet energy scale in CMS with pp collisions at $\sqrt{s}$=7 TeV*. CMS Physics Analysis Summary **CMS-PAS-JME-10-010** (2010).

[30] CMS Collaboration. *Absolute Calibration of the Luminosity Measurement at CMS: Winter2012 Update*. CMS PAS **SMP-12-008** (2012).

[31] *Performance of the b-jet identification in CMS*. CMS Physics Analysis Summary **CMS-PAS-BTV-11-001** (2011).

[32] The ATLAS. *Procedure for the LHC Higgs boson search combination in Summer 2011*. Technical Report CMS-NOTE-2011-005 CERN Geneva Aug 2011.

[33] S. Heinemeyer, W. Hollik and G. Weiglein. *FeynHiggs: A program for the calculation of the masses of the neutral CP-even Higgs bosons in the MSSM*. Comput. Phys. Commun. **124**, 76–89 (2000).